conductor film. This indicates that the loss mechanism, such as recombination, normally encountered in semiconductor photoelectrochemistry, has been minimized. The performance characteristics achieved here are comparable to those of high quality single crystal photovoltaic cells. The conversion efficiency is the maximum power output expressed as a percentage of the input light power

$$\eta(\%) = \text{maximum output power} \times 100/(\text{irradiance} \times \text{area})$$

Figure 5 gives $\eta = 12\%$ for 470-nm light which is by far the highest monochromatic conversion yield achieved until now in dye sensitized regenerative photoelectrochemical cells. The maximum monochromatic efficiency reported previously by Matsumara et al.[4] is 2.5% for 540-nm light and sintered ZnO pellets coated with rose bengal as a sensitizer.

We finally report preliminary findings obtained with the RuL_3^{4-}-sensitized regenerative cell by using polychromatic light excitation. The conditions used were the same as in Figure 5 except that the concentration of LiBr was 0.1 M and that the entire $\lambda > 420$ nm light output of the high pressure Xe lamp was used for excitation of the RuL^{4-}-coated 2×2 cm sized TiO_2 film. The light power incident on the 4 cm^2 TiO_2 sheet was 174 mW. Open circuit voltage was 0.92 V, and the short circuit current was 3.4 mÅ. Maximum power output was 2.1 mW at a cell voltage of around 0.73 V corresponding to a fill factor of 0.67 and a conversion efficiency of 1.2%. Decreasing the incident power by a factor of 10 resulted in an increase of η to 1.6%. These performance parameters may be further improved by optimizing the experimental conditions. Also, it should be noted that polychromatic efficiencies depend on the emission features of the light source. Sunlight experiments will provide the solar conversion characteristics.

Conclusions

The findings presented here confirm the very promising properties of high surface area anatase films employed in conjunction with suitable sensitizers, as visible light energy harvesting and conversion devices. RuL_3^{4-}-coated films display incident monochromatic photon to current conversion efficiencies of up to 74%. Turnover numbers exceeding several 10 000 show the extremely rugged character of this chromophore, the quantum yield for destructive side reactions being below 10^{-5}. Another attractive feature of RuL_3^{4-} is the high redox potential in the ground state allowing the sensitized electron injection in the semiconductor to be coupled to thermodynamically demanding oxidation reactions. The present report focusses on the oxidation of halide ion. For the first time the sensitized generation of Br_2 from Br^- is achieved at a large band gap semiconductor electrode. This reaction is exploited to generate electrical power in a photodriven electrochemical cell. Even without optimization, a monochromatic conversion efficiency as high as 12% and a fill factor of 0.74 have been obtained. Due to their durability, low cost, and high efficiency these systems appear to have the potential to serve in practical solar energy conversion devices.

Acknowledgment. This work was supported by the Gas Research Institute, Chicago, IL (subcontract with the Solar Energy Research Institute (SERI), Golden, CO), the Swiss National Energy Foundation (NEFF), and the Swiss Office for Energy (OFEN). We are grateful to Dr. Ersi Vrachnou for assistance with the chemical actinometry. We also acknowledge discussions with Prof. Martin Fleischmann, University of Southampton, U.K., concerning the fractal character of the TiO_2 film.

Registry No. RuL_3^{4-}, 78338-26-8; TiO_2, 13463-67-7; Br_2, 7726-95-6; LiBr, 7550-35-8; KI, 7681-11-0; NaBr, 7647-15-6; $HClO_4$, 7601-90-3; hydroquinone, 123-31-9.

Structural Effect of *gem*-6 Substitution on C, N, P, S, and O Atoms: Crystallographic Data Analysis of Numerous C_3CZCC_3 Fragments. Modelization of Static and Dynamic Molecular States

Jacques-Emile Dubois* and Aliette Cossé-Barbi

Contribution from the Institut de Topologie et de Dynamique des Systèmes de l'Université Paris 7, Associé au CNRS, 1, Rue Guy de la Brosse, 75005 Paris, France. *Received July 10, 1985. Revised Manuscript Received September 19, 1987*

Abstract: C_3CZCC_3 fragments show systematic distortions of local symmetries when compared with structures chosen as formal references. Interactions between groups lead the structure to search for stable shapes by complex processes involving both *rotational* and *framework distortions*. In acyclic series tertiary groups avoid each other by a conrotatory rotational process (static gear effect), while in cyclic series (six-membered ring) the process is disrotatory and the twist conformers are forbidden. In the conformational ϕ_1, ϕ_2 mean torsion angle space, this leads to an *impressive sectorization of acyclic fragments in quadrants 1 and 3* ($\phi_1 \times \phi_2 > 0$) *and cyclic ones in quadrants 2 and 4* ($\phi_1 \times \phi_2 < 0$). Framework distortions (FRAM.DST.) are distributed throughout the entire fragment. They involve a significant opening of angle CZC (CZC BEND.), the symmetrical deformation of C_3C groups by contraction or expansion, and the C_3C tilt. Thus, four basic strain release effects (ROT.DST., CZC BEND., CC_3 SYM.DEF., CC_3 TILT) exist in all the subclasses examined (Z = C_{sp^3}, C_{sp^2}, NO, NH, NMe, P, cyclic, or acyclic fragments) with different amplitudes. They are *interdependent* among themselves and are a function of the hybridization of the Z atom. In each subpopulation, their mean value provides a basis for *predicting* new strain geometries. Correlated rotations and CZC bending are equally efficient in reabsorbing steric energy (MM simulation in a model compound). Any one of these two effects without the other accounts for some two-thirds of the steric strain release at the most. Despite crowding, the conformational flexibility of C_3CZCC_3 fragments remains considerable. Their shape variations are dynamically associated with some framework deformation steps all along the interconversion pathways. Thus, the smaller apparent size of tertiary groups results from the *cooperative interaction* of framework distortions and specific rotational processes, the former lowering the energy barriers (from several hundred to several kilocalories/mole; INDO and MM calculations) of the interconversion pathways forbidden with standardized molecular frameworks.

Crowded systems, in particular those with two tertiary groups in *gem* position, have certain specificities that have been approached in two different ways: studying property variations in families by progressive substitution and comparing C_3CZCC_3

0002-7863/88/1510-1220$01.50/0

Table I. *gem* Substitution of a Z Atom by Two Tertiary Groups and Additivity Deviation: $n \rightarrow \pi^*$ Transition and C=O Stretching Wavenumbers, ν (cm^{-1}); Chemical Shift, δ; Formation Enthalpy ΔH_f^0 (kcal·mol^{-1}) (Minus, Attenuation with Regard to the Expected Substitution Effect; Plus, Heightening)

Acyclic Compounds

	Z = C						Z = O,	Z = S	
	ketones (RCOR′)					thioketones (RCSR′)	ethers (ROR′)	sulfoxides (RSOR′)	sulfones (RSO_2R')
technique	$\nu_{n\rightarrow\pi^*}$[3]	$\nu_{C=O}$[1,2]	$\delta_{^{13}C}$[4,5]	$\delta_{^{17}O}$[6]	ΔH_f^0[7]	$\delta_{^{13}C}$[9]	$\delta_{^{13}C}$[10]	$\delta_{^{17}O}$[11]	$\delta_{^{17}O}$[11]
deviation	400	13	−2.3	−21.5	−7.2	−2.2	−12.5	−34[a]	−24[a]

Cyclic Compounds

	Z = C		Z = N,
	cyclohexanones	cyclohexanes	piperidines
technique	$\nu_{n\rightarrow\pi^*}$[3]	$\delta_{^{13}C}$[12]	$\delta_{^{15}N}$[13]
deviation	600	−3.1	−9.4

[a] Anomaly calculated with regard to an average effect of the Me groups deduced from Me-Z-Me, Et-Z-Et, *i*-Pr-Z-*i*-Pr.

fragments of comparable strain.

The first approach involves the spectroscopic properties IR,[1,2] UV,[1,3] and NMR[4-6,8-13] and thermodynamics.[7] These properties reveal the existence of an anomaly or *gem*-6 effect associated with the passage from the fifth (*t*-Bu-Z-*i*-Pr) to the sixth substitution (*t*-Bu-Z-*t*-Bu) in various series of acyclic compounds (ketones,[1-7] alkenes,[8] alcohols,[8] alkanes,[8] thioketones,[9] ethers,[10] sulfoxides,[11] and sulfones[11]) or cyclic compounds (cyclohexanones,[3] cyclohexanes,[12] and piperidines[13]) (Table I). Reactivity studies on series of increasingly substituted compounds show specific effects on rates and mechanisms and lead to the notion of an *apparent size* of tertiary groups reduced in compounds where two such groups are geminal.[14]

By comparing 23 acyclic crystallographic fragments C_3CCCC_3 of comparable strain, Mislow et al. showed the existence of gear-meshed ground-state structures and particular interconversion mechanisms giving rise to the correlated rotation of tertiary groups.[15] The apparent reduced size of the tertiary groups could then be explained by the lessening of their mutual interactions without framework deformation. Nonetheless, the *gem*-6 effect of ketones,[3,18] sulfoxides,[16] and phosphines[17] is interpreted on the basis of a large valency opening of angle CZC (Z = C, S, P) of C_3CZCC_3 fragments.

Does a specific rotational mechanism, such as the gear effect[19] exist in all series of compounds with *gem*-6 exceptional behavior (cyclic and acyclic compounds; Z = S, O, N, P)? If so, can this alone explain all the *apparent size limitations* of tertiary groups, or is it linked to framework distortions acting in the same direction? This concept of apparent size should then be reexamined in the light of real molecular sizes.

In this study we analyze the crystallographic data for 239 acyclic and cyclic (six-membered rings) C_3CZCC_3 fragments with a Z atom (carbon or heteroatom) *gem* substituted by two tertiary groups. Their shapes are described in terms of local symmetry coordinates.[20] The parameters, valency angles and bond lengths, are compared with those observed in corresponding little-substituted compounds CH_3CZCH_3..., in which the steric interactions (bond–bond and atom–atom interactions[21]) are recognized as weak (section I). We deduce four basic effects for strain adaptation of fragments C_3CCCC_3 (section II) and C_3CZCC_3 (Z = P, N, O, S, Si) (section III) and calculate their efficiencies with regard to steric energy resorption. By studying interconversion pathways and theoretically evaluating rotation barriers (section IV), we can approach the problem of apparent size as related to framework distortion.

I. Methods

I.1. Interrogating the Structural Bank. (a) Data Selection. The experimental data used in our analysis were taken from the Cambridge Crystallographic Data Base[22] updated in January 1983.

The connectivity search selects structures containing C_3CZCC_3 fragments. CC_3 tertiary groups are not necessarily *t*-Bu groups; any substitutions (* in diagrams 1 and 2) can appear on carbon atoms 1 and 5–9.

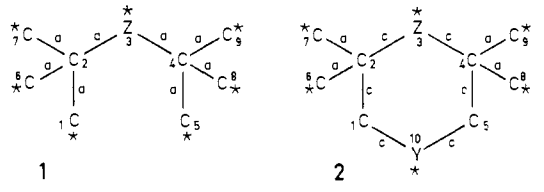

1 2

The Z atom can also carry substituents. All the bonds of the fragment C_3CZCC_3, i.e., those detailed in diagrams 1 and 2, are single. They can be acyclic; the substructure sought for then corresponds to diagram 1.

(1) Maroni, P.; Dubois, J. E. *J. Chim. Phys.* **1954**, *402*, 51.
(2) Massat, A.; Dubois, J. E. *J. Mol. Struct.* **1969**, *4*, 385. Dubois, J. E.; Massat, A.; Guillaume, Ph. *J. Mol. Struct.* **1969**, *4*, 402.
(3) Cossé-Barbi, A. *C.R. Hebd. Seances Acad. Sci.* **1971**, *273*, 380. *J. Chim. Phys.* **1979**, *5*, 76 and references therein.
(4) Jackman, L. M.; Kelly, D. P. *J. Chem. Soc. B* **1970**, 102.
(5) Dubois, J. E.; Doucet, J. P.; Tiffon, B. *J. Chim. Phys.* **1973**, 805. Dubois, J. E.; Carabédian, M. *Org. Magn. Reson.* **1980**, *14*, 264.
(6) Delseth, Cl.; Kintzinger, J. P. *Helv. Chim. Acta* **1976**, *59*, 466; **1976**, *58*, 1410.
(7) Dubois, J. E.; Herzog, H. *J. Chem. Soc., Chem. Commun.* **1972**, 932.
(8) Panaye, A.; Doucet, J. P.; Dubois, J. E. *Tetrahedron Lett.* **1981**, *22*, 1235. Doucet, J. P.; Panaye, A.; Dubois, J. E. *J. Org. Chem.* **1983**, *48*, 3174.
(9) Andrieu, Cl. G.; Debruyne, D.; Paquer, D. *Org. Magn. Reson.* **1978**, *11*, 528.
(10) Delseth, Cl.; Kintzinger, J. P. *Helv. Chim. Acta* **1978**, *61*, 1327.
(11) Dyer, J. C.; Harris, D. L.; Evans, S. A. *J. Org. Chem.* **1982**, *47*, 3660.
(12) Dalming, D. K.; Grant, D. M. *J. Am. Chem. Soc.* **1967**, *89*, 6612; **1972**, *94*, 5218; **1973**, *95*, 3718. Maciel, G. E.; Dorn, H. C. *Org. Magn. Reson.* **1974**, *6*, 178; *J. Am. Chem. Soc.* **1971**, *93*, 1268.
(13) Duthaler, D. O.; Williamson, K. L.; Giannini, D. D.; Bearden, W. H.; Roberts, J. D. *J. Am. Chem. Soc.* **1977**, *99*, 8406. Ellis, G.; Jones, R. G. *J. Chem. Soc., Perkin Trans. 2* **1972**, 437. See also the ^{15}N chemical shift of piperidine hydrochlorides: Duthaler, R. O.; Roberts, J. D. *J. Am. Chem. Soc.* **1978**, *100*, 3882.
(14) Berg, U.; Liljefors, T.; Roussel, C.; Sandström, J. *Acc. Chem. Res.* **1985**, *18*, 80 and references therein.
(15) Nachbar, R. B.; Johnson, C. A.; Mislow, K. *J. Org. Chem.* **1982**, *47*, 4829.
(16) Bock, H.; Solouki, B. *Angew. Chem., Int. Ed. Engl.* **1972**, *11*, 436.
(17) Bel'skii, V. E.; Romanov, G. V.; Pozhidaev, V. M.; Pudovik, A. N. *Zh. Obshch. Khim.* **1977**, *80*, 1222.
(18) Dubois, J. E. *Pure Appl. Chem.* **1977**, *49*, 1029. Cossé-Barbi, A. *J. Mol. Struct.* **1978**, *49*, 181.
(19) For a definition of static and dynamic gear effects, see: (a) Hounshell, W. D.; Iroff, L. D.; Iverson, D. J.; Wroczynski, R. J.; Mislow, K. *Isr. J. Chem.* **1980**, *20*, 65. (b) Roussel, C.; Chanon, M.; Metzger, J. *Tetrahedron Lett.* **1971**, 1861. Roussei, C.; Liden, A.; Chanon, M.; Metzger, J.; Sandström, J. *J. Am. Chem. Soc.* **1976**, *98*, 3847.
(20) Murray-Rust, P.; Bürgi, H. B.; Dunitz, J. D. *Acta Crsytallogr., Sect. A: Cryst. Phys. Diffr. Theor. Gen. Crystallogr.* **1979**, *35*, 703.
(21) Pitzer, R. M. *Acc. Chem. Res.* **1983**, *16*, 207.
(22) Allen, F. H.; Bellard, S.; Brice, M. D.; Cartwright, B. A.; Doubleday, A.; Higgs, H.; Hummelink, T.; Hummelink-Peters, B.; Kennard, O.; Motherwell, W. D. S.; Rodgers, J. R.; Watson, D. G. *Acta Crystallogr., Sect. B: Struct. Crystallogr. Cryst. Chem.* **1979**, *35*, 2331. Wilson, S. R.; Huffman, J. C. *J. Org. Chem.* **1980**, *45*, 560.

Chart I. Internal Coordinates

CZC Unit

$23 = r_1$	$234 = \theta$
$34 = r_2$	

C_3C- Rotors

$12 = r_1'$	$123 = \beta_1$	$627 = \alpha_1$	$1234 = \omega_1$
$26 = r_2'$	$623 = \beta_2$	$127 = \alpha_2$	$6234 = \omega_2$
$27 = r_3'$	$723 = \beta_3$	$126 = \alpha_3$	$7234 = \omega_3$
$45 = r_4'$	$345 = \beta_4$	$849 = \alpha_4$	$2345 = \omega_4$
$48 = r_5'$	$348 = \beta_5$	$549 = \alpha_5$	$2348 = \omega_5$
$49 = r_6'$	$349 = \beta_6$	$548 = \alpha_6$	$2349 = \omega_6$

Four of them (12, 23, 34, 45) can be integrated into a six-membered ring, while the others are acyclic; the substructure sought for then is 2. The Y atom can be any atom and can carry substituents: the 1,10- and 5,10-bonds are single.

This selection results in 88 hits for the acyclic substructure 1 and 66 hits for the cyclic substructure 2. Of these 154 hits, 34 cannot be used because the atomic coordinates are not stored. We thus obtain 120 hits containing 239 fragments (163 times substructure 1 and 76 times substructure 2). Of these 239 fragments, 24 are not used because of unreliable (flag error) or too imprecise atomic coordinates ($R > 0.15$).

The disordered fragments obtained with the desired precision (there are five) are reported in the figures. Although they are not included when calculating averages, they are valuable for pointing out structural, and in particular conformational, variability.

The study includes 108 compounds (110 if we count disordered C_3CZCC_3 fragment compounds), containing 210 fragments (or 215). Of these, 67 fragments are cyclic and 143 (or 148) acyclic. The Z atoms are C (50 or 55), P (108), N (42), Si (3), S (3), O (3), and Sn (1). These include 23 acyclic fragments studied in a previous work by Nachbar, Johnson, and Mislow.[15]

Associated bibliographic and crystallographic information is summarized in the supplementary material.

(b) Division into Subclasses. Data have been subdivided according to the nature of the Z atom. The discussion pays attention to those subgroups containing a large number of fragments (Z = C, N, P): compounds related to di-*tert*-butylmethane and 1,1,3,3-tetramethylcyclohexane (Z = C, 55 fragments), 2,2,6,6-tetramethylpiperidine (Z = N, 42 fragments), and di-*tert*-butylphosphine (Z = P, 108 fragments).

A finer subdivision is based on the nature of the other substituent atoms of atom Z. In this way, we differentiated between carbons sp^3 and sp^2 and noted the compounds related to 2,2,4,4-tetramethylpentane and exhibiting a ketone function, nitrile, or a methylene group in position 3, as well as those related to 1,1,3,3-tetramethylcyclohexane and exhibiting a ketone function, nitrile, or a thiocarbonyl in position 2. $(C_3C)_3P$ and $(C_3C)_4P$ fragments are studied apart. The derivatives of 2,2,6,6-tetramethylpiperine, 2,2,6,6-tetramethylpiperidine-1-oxyl, or 2,2,6,6-tetramethylpiperidine-1-sulfenyl, -sulfonyl, or -sulfinyl are analyzed separately.

Eight of the 148 acyclic fragments have substituents on at least one of the carbons 1 and 5–9. Of the 67 cyclic fragments, 8 have substituents on at least one of the carbons 6–9. These fragments were carefully compared with those without such substitutions.

(c) Geometric Calculation. The calculated internal coordinates are given in Chart I.

I.2. Shape Description and Strain Perturbation. The shape of a fragment is entirely known by the set of its 27 internal coordinates, but simply observing the coordinate table or the resulting image (graphic) does not reveal the secrets of the shape. The shape can be analyzed only by being compared with other more familiar shapes with ideal symmetries and standard metrics.

(a) Local Symmetry Coordinates. We associate a set of 21 linearly independent symmetry distortion coordinates[20] to these 27 internal coordinates.. The shape is described with regard to a more symmetrical ideal structure (gear-clashed structure) with C_{2v} symmetry of unit CZC, C_{3v} symmetry of tertiary groups CC_3, and global C_{2v} symmetry of fragment C_3CZCC_3. We have chosen the following distortion coordinates in order to describe shape.

Global C_{2v} symmetry (two coordinates): $S_1 = \phi_1 + \phi_2$ and $S_2 = \phi_1 - \phi_2$, with $\phi_1 = (\omega_1 + \omega_2 + \omega_3 - 180°)/3$, $\phi_2 = (\omega_4 + \omega_5 + \omega_6 - 180°)/3$, $-180° < \omega_i \leq 180°$, $|\omega_1| \leq |\omega_2| < |\omega_3|$, and similar conditions for ω_4, ω_5, ω_6.

The two coordinates S_1 and S_2 represent the conrotatory (S_1) and disrotatory (S_2) correlated rotation of the two tertiary groups.

The bidimensional space defined by ϕ_1, ϕ_2 or, similarly, by S_1, S_2 provides an image of stable and unstable conformers and enables us to describe their interconversion. This point was amply developed elsewhere.[23] The ϕ_1, ϕ_2 space symmetry is isomorphic to group G_{36}, and a cell measuring (360° × 360°)/36 suffices to group all the available information. Figures 1, 4, and 6, limited to a conformational space measuring (360° × 360°)/9, contain four equivalent cells. A fragment is shown by four equivalent coordinate points (ϕ_1, ϕ_2), $(-\phi_1, -\phi_2)$, $(-\phi_1, \phi_2)$, and $(\phi_1, -\phi_2)$. These are deduced from each other by symmetries with regard to the center of the coordinate system and to the axes S_1, S_2.

Local C_{2v} symmetry of unit CZC (three coordinates): $S_1' = \theta$, CZC bending; $S_2' = r_1 + r_2$, CZ symmetrical stretch; $S_3' = r_1 - r_2$, CZ asymmetrical stretch.

Local C_{3v} symmetry of each C_3C unit (8 × 2 linearly independent coordinates): $S_3 = 2\omega_1 - \omega_2 - \omega_3$ and $S_4 = \omega_2 - \omega_3 - 120°$, C_3C rotational asymmetry; $S_4' = \beta_1 + \beta_2 + \beta_3 - \alpha_1 - \alpha_2 - \alpha_3$, symmetrical C_3C deformation; $S_5' = 2\beta_i - \beta_j - \beta_k$, "in plane" C_3C rock; $S_6' = \beta_j - \beta_k$, "out of plane" C_3C rock; $2\alpha_1 - \alpha_2 - \alpha_3$, redundant; $\alpha_2 - \alpha_3$, redundant; $\alpha_1 + \alpha_2 + \alpha_3 + \beta_1 + \beta_2 + \beta_3$, redundant; $S_7' = r_1' + r_2' + r_3'$, CC symmetrical stretch; $S_8' = 2r_1' - r_2' - r_3'$ and $S_9' = r_2' - r_3'$, CC asymmetrical stretch.

From these 11 symmetry distortion coordinates, 3 are redundant; 8 other linearly independent coordinates S_5, S_6, S_{10}'–S_{15}' are similarly defined for the other C_3–C rotor.[24]

Theoretically, to describe rocking, we need two coordinates. In reality, among the three systems of mathematically equivalent coordinates constructed with $i, j, k = 1, 2$, or 3 and $i \neq j \neq k$, there is almost always a system for which the out-of-plane rocking coordinate is weak. We then obtain a satisfactory description of the rocking by setting aside this out-of-plane C_3C rocking coordinate. The rocking takes place in the CCZ plane defined by the ω_i torsion angle.

(b) Formal References. Symmetry coordinates fall into two categories: (1) Those that translate distortion with regard to C_{2v} and C_{3v} local symmetries or with regard to C_{2v} global symmetry; there are asymmetrical CZ stretch (S_3'), rotational C_3C asymmetry (S_3, S_4, S_5, S_6), in-plane and out-of-plane rock (S_5', S_6', S_{11}', S_{12}'), asymmetrical CC stretch (S_8', S_9', S_{14}', S_{15}'), and the S_1 and S_2 conrotatory and disrotatory coordinates. (2) Those that do not translate distortion with regard to local or global symmetries (CZC bending S_1', CZ symmetrical stretch S_2', symmetrical C_3C deformations S_4' and S_{10}', symmetrical CC stretch S_7' and S_{13}').

For example, in fragments C_3CZCC_3 with Z = C_{sp^3}, the CZC angle (120.7°) is very different from the CZC angle seen in fragments CH_3 C_{sp^3} CH_3 (112.80°). This heightened value, although respecting the C_{2v} symmetry of the fragment, indicates the importance of the tension inside the *gem*-6 structure. It can be viewed as an element of the *gem*-6 structure adaptation to the importance of these tensions.

It seemed then useful to evaluate the distortions as compared with "formal" or "standard" structural elements extracted from little-substituted systems wherein tensions are weak.

These formal references are the standard gear-clashed structures whose characteristics are those of nonsubstituted systems mentioned below: CZC bond angles and CZ bond lengths equal to those of acyclic compounds CH_3CZCH_3 or cyclic compounds $(CH_2)_5Z$;[25] CC bond lengths of C_3C- rotors equal to those of fragments CH_2–CH_2–Z..., cyclic or acyclic; angles α_i and β_i equal to their standard value in CH_4 (109°28′); torsion angles ω_i equal to 180, 60, or −60°.

I.3. MO and MM Calculations. For conformational calculations, we use the INDO method.[26] A first approach of potential wells and of low-energy zones is obtained on a standardized geometry by a study of hypersurface E (ϕ_1, ϕ_2) describing energy with regard to two torsion angles ϕ_1, ϕ_2 and to associated level lines. These proceed by 5-deg steps on ϕ_i angles. The conformational map is refined by simultaneous optimizing of the function E (ϕ_1, ϕ_2) on some 20 internal coordinates.[27] By filtering energy, smaller than a threshold value, that we cause to vary gradually, we visualize interconversion pathways.

Steric energy is calculated by molecular mechanics (MM2 program).[28] Steric energy here is the difference between the energy of the *molecular entity being studied* and that of a *hypothetical entity*, where all the internal coordinate values are equal to the reference value of this method.

(23) Bürgi, H. B.; Hounshell, W. D.; Nachbar, R. B.; Mislow, K. *J. Am. Chem. Soc.* **1983**, *105*, 1427.

(24) For rotors C_3C-, it was possible to choose the symmetry coordinates associated with the irreducible representations A_1, A_2, B_1, B_2 of the C_{2v} group. We preferred to emphasize the local distortion of each C_3C- group rather than eventual symmetry relations between the two C_3C groups. Bürgi and coworkers made the same choice formerly[23] for the S_3, S_4, S_5, S_6 coordinates associated with the torsion angles.

(25) References in the Cambridge Data Base are not always the ideal ones. We retained the fragments closest to the ideal and controlled parameter values by comparing them with those measured in vapor phase for ideal compounds whenever available.

(26) Pople, J. A.; Beveridge, D. L.; Dobosh, P. A. *J. Chem. Phys.* **1967**, *47*, 2026.

(27) Rinaldi, D.; Rivail, J. L. *C.R. Hebd. Sceances. Acad. Sci. Ser.* **1972**, *274*, 1664.

(28) Allinger, N. L. *J. Am. Chem. Soc.* **1977**, *99*, 8127.

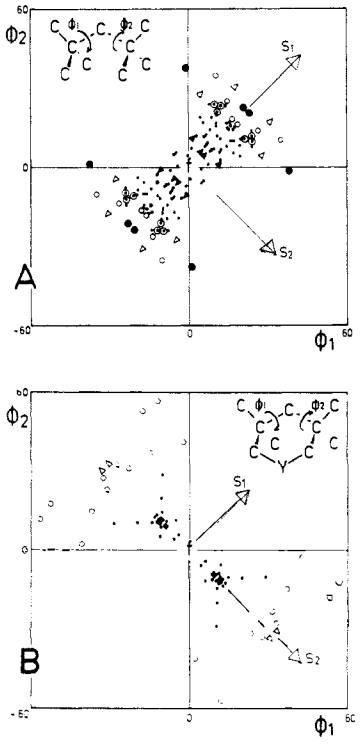

Figure 1. Rotational distortion from gear-clashed reference f leading to a quadrant sectorization (Z = C). A, acyclic fragments, sectorization in quadrants 1 and 3 (ϕ_1 and ϕ_2 of the same sign); a disordered fragment outside the sector belongs to compound **18** of the supplementary material. B, cyclic fragments, sectorization in quadrants 2 and 4 (ϕ_1 and ϕ_2 of opposite signs). Z = C_{sp^2} (○); Z = C_{sp^3} (·); disordered fragments, C_{sp^2} (●), C_{sp^3} (⊙); fragments with substitutions on one or several carbons of substructures 1 or 2, C_{sp^2} (△), C_{sp^3} (▲).

II. Analyzing the Crystallographic Data of Fragments C_3CCCC_3—Strain Release Effects

The strain release effects are presented as rotational effects and framework distortion effects.

II.1. Rotational Distortions. (a) Quadrant Sectorization. In spite of the remarkable heterogeneity of the substituents of Z atoms, a fairly pronounced conformational regularity is discernible (Figure 1). Two different situations occur for acyclic and cyclic fragments. The corresponding points group themselves in quadrants 1 and 3 ($\phi_1 \times \phi_2 > 0$) or in quadrants 2 and 4 ($\phi_1 \times \phi_2 < 0$) and induce a quadrant sectorization.

When the compound is acyclic (Figure 1A), the representative points are inscribed in quadrants 1 and 3, corresponding to mean torsion angles ϕ_1 and ϕ_2 of the same sign. The corresponding gear-meshed structures are thus generated by conrotation from the references, gear-clashed[19] structures of C_{2v} local symmetry ($\phi_1 = \phi_2 = 0$) (Figure 2). They avoid 1–5 and 6–8 synaxial interactions. However, conrotation is rarely symmetrical (S_1) and includes a part of component S_2; the resulting gear-meshed structures thus separate themselves from C_2 local symmetry.

When the compound exhibits a six-membered ring (Figure 1B), nearly all the representative points are inscribed in quadrants 2 and 4, corresponding to mean torsion angles of opposite signs. The corresponding structures are thus generated by disrotation from their chair structures ($\phi_1 = \phi_2 = 0$) (Figure 2).

The static gear effect shown in acyclic fragments is thus not found in six-membered rings. In these crowded structures, very flattened chair and boat shapes are observed; the closing of the cycle introduces a specific constraint forbidding the conrotatory process and, consequently, the twisted shapes that would be localized in quadrants 1 and 3.

This disrotation, often symmetrical and represented then exclusively by the component S_2, leads to structures endowed with C_s local symmetry (Figure 2). Thus, disrotation transforms the standard constrained gear-clashed structure into another structure of the same type but with less 6–8 synaxial interaction.

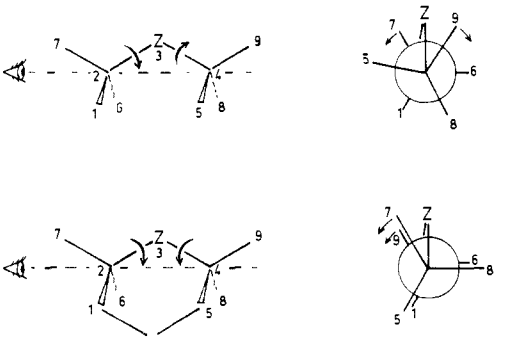

Figure 2. Strain limitation in standard gear-clashed geometries (on the left): by conrotation, leading to an intermeshed gear structure of local C_2 symmetry, above; by disrotation, leading to a less constrained gear-clashed structure of local C_s symmetry, below.

We draw away from the mechanical gear analogy.[19a] In mechanical systems, the two cogwheels have parallel axes and all the gear-clashed situations are equally strained. Here, with molecular systems, the strain release is obtained by symmetrical disrotation because the rotation axes are not parallel.

(b) Range of Rotational Processes and Z Hybridization. The range of rotational processes of strain release can be measured by distance $(\phi_1^2 + \phi_2^2)^{1/2}$. It varies according to the compound. These processes, whether mainly conrotatory (acyclic series) or disrotatory (cyclic series), can be especially broad if the Z atom is an sp^2 rather than an sp^3 carbon. Of particular interest for interpreting this fact are the following: (1) The internal rotation barrier around 2–3 and 3–4 bonds. This is weaker for a rotation around a C_{sp^2}–C_{sp^3} ($\simeq$1 kcal·mol^{-1}) than for a rotation around a C_{sp^3}–C_{sp^3} ($\simeq$3 kcal·mol^{-1}). Thus, the syn axial steric interactions can be more easily minimized by varying the torsion angles (i.e., at the cost of internal torsion energy) if Z = C_{sp^2} rather than C_{sp^3}. (2) The role of steric interactions (--- in diagrams 3 and 4), bond–bond and atom–atom, resulting from the proximity of Z atom substituents and equatorial groups 7 and 9. In gear-clashed

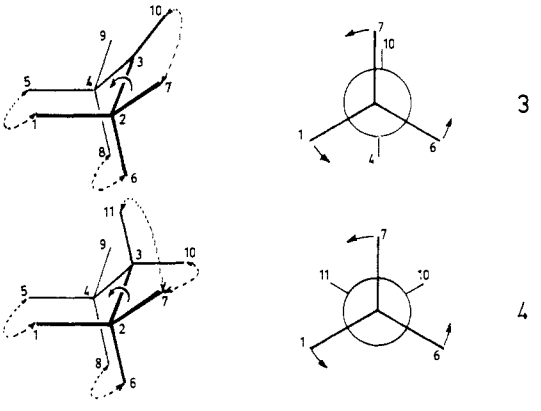

references, these interactions are larger when the carbon is sp^2 instead of sp^3 (3 compared with 4). The rotation also helps lessen this interaction when the Z atom is C_{sp^2}, whereas a very strong rotation ($\simeq$30°) would increase it if Z = C_{sp^3}.

These are two versions of the same interpretation. We must recall that the internal rotation barrier is linked to the existence of primarily bond–bond interactions[21,29] acting in opposite directions when Z = C_{sp^2} (3). On the contrary, their effect on the barrier is cumulative when Z = C_{sp^3} (4).

(c) Rotational Asymmetry of C_3C–Z Rotors. Analysis of the conformational space built on mean torsion angles ϕ_1 and ϕ_2 does not include the specific rotational asymmetry of tertiary groups. This distortion exists when the dihedral angles between the three ZCC planes of the rotor are other than 120°.

S_3, S_4, S_5, S_6 parameters of rotational asymmetry prove to be moderate (Table II). The rotational asymmetry of C_3C–Z rotors

(29) Wiberg, K. B.; Martin, E. *J. Am. Chem. Soc.* **1985**, *107*, 5035.

Table II. Range of Strain Release Conrotatory or Disrotatory Mechanisms (Standard Deviation σ in Parentheses) and Rotational Asymmetry Parameters of C_3C– Rotors (Average Values in Degrees)

	acyclic fragment, Z				cyclic fragment, Z						
	C_{sp^3}	C_{sp^2}	P	Si	C_{sp^3}	C_{sp^2}	NH, NMe	NS	NO	S	O
$\phi = ((\phi^2_1 + \phi^2_2)/2)^{1/2}$	11.0	20.2	14.1[a]	12.5	11.7	27.6	18.5	21.3	28.2	20.7	11.5
σ	(4)	(4)	(4)	(8)	(4)	(11)	(9)	(12)	(6)	(4)	(4)
$\lvert 2\omega_1 - \omega_2 - \omega_3\rvert$, $\lvert 2\omega_4 - \omega_5 - \omega_6\rvert$	1.9	0.2	0.9	0.4	2.6	3.3	3.6	5.1	0.5	0.5	1.9
$\lvert \omega_2 - \omega_3\rvert$, $\lvert \omega_5 - \omega_6\rvert$	3.7	3.4	2.6	2.7	2.3	0.3	3.7	2.8	1.3	4.8	4.1

[a] $(C_3C)_3P$ fragments: 14.84.

Table III. CZC Unit Perturbation Measured by Comparison with Formal References (CZC Bending in Degrees, CZ Symmetrical and Asymmetrical Stretch in Angstroms; Mean Values, Standard Deviation in Parentheses)

	acyclic fragment, Z				cyclic fragment, Z						
	C_{sp^3}	C_{sp^2}	P	Si	C_{sp^3}	C_{sp^2}	NH, NMe	NS	NO	S	O
θ	8.6	5.2	10.5[a]	12.3	7.5	3.9	6.3	6.4	11.0	7.1	9.7
	(2.2)	(3.3)	(2.3)	(0.3)	(2.1)	(1.4)	(1.4)	(0.7)	(2.5)	(0.4)	(0.5)
$(r_1 + r_2)/2$	–0.004	0.028	0.042[a]	0	0.022	0.041	–0.006	0.047	0.013	0.027	0.065
	(0.021)	(0.027)	(0.032)	(0.058)	(0.031)	(0.014)	(0.018)	(0.020)	(0.019)	(0.002)	(0.047)
$(r_1 - r_2)$	0.014	0.022	0.021[a]	0.013	0.026	0.003	0.007	0.020	0.001	0.0005	0.036
	(0.010)	(0.015)	(0.019)	(0.007)	(0.026)	(0.005)	(0.008)	(0.025)	(0.008)	(0.0007)	(0.051)

[a] $(C_3C)_3P$ and $(C_3C)_4P$ fragments excluded. For the former, mean CZC and symmetrical CZ stretching values are 6.80° and 0.079 Å.

can be negligible with a good approximation.

II.2. Frame Distortions. A wide scattering of data concerning bond angles and bond lengths is observed so that a precise generic *gem*-6 framework is difficult to define.

We note, however, some interesting regularities concerning the CZC unit as well as C_3C– rotors.

(a) CZC Unit (Table III). Valency angle distortions are more important than bond length distortions. The mean CZ distance (coordinate $r_1 + r_2$) is similar to that observed for corresponding nonsubstituted compounds ($Z = C_{sp^3}$). We observe a slight but systematic elongation of the distances for $Z = C_{sp^2}$ in cyclic series.

The inequality of CZ distances (coordinate $r_1 - r_2$) can be great. It is, however, not larger than 0.026 Å (C_{sp^3}; cyclic fragments, i.e., an average of 1.6% in relative value).

The angle CZC (S_1' coordinate) has a much larger value than that observed for corresponding nonsubstituted compounds.

Although the most important effect is the CZC bending (CZC BEND.), this opening tends to be heightened for short CZ distances. On the other hand, the CZC opening is much greater if the carbon is sp^3 instead of sp^2. It should indicate only that the bending constant is smaller for an sp^3 than sp^2 carbon. But, vibrational analysis of analogous compounds[30] shows us that the bending constants are similar. This indicates a competition between two strain release mechanisms, the rotational process and the central angle deformation. Syn axial interactions cannot be limited easily at the cost of the internal torsion energy for $Z = C_{sp^3}$, because of the barrier height. This is done then at the cost of the bending energy.

(b) C_3C Unit (Table IV). As for the unit CZC, bond angles are more distorted here than bond lengths. Angle effects are more preponderant for $Z = C_{sp^3}$ than for $Z = C_{sp^2}$.

Unequal β_i (ZCC) angles are the rule, and their average value is always different from 109°28′.

The inequality of β_i angles indicates *C_3C rocking*. The approximate threefold axis of the tertiary group does not point along the CZ bond direction but deviates from it systematically (Figure 3b). This symmetry axis deviation is similar to the methyl tilt observed in little-substituted compounds (MeOH, $MeNH_2$, MeNO, MeSH).[31]

In acyclic series, this C_3C tilt or rocking is linked to a *reduced real size of the C_3C group by contraction* (CC_3 SYM.DEF., S_4'): α_i angles (CCC) become narrower, while β_i angles open globally (Figure 3c). In cyclic series the contraction is attenuated.

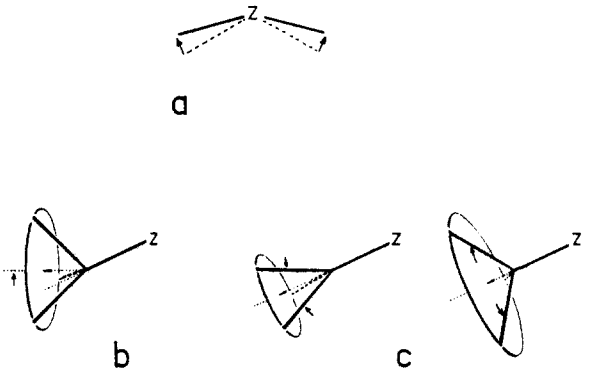

Figure 3. Bond angle distortions: CZC opening (a), C_3C rocking (b), CC_3-symmetrical deformation by contraction or expansion (c).

Table IV. C_3C Symmetrical Deformation by Contraction ($\sum\beta - \sum\alpha > 0$) or Expansion ($\sum\beta - \sum\alpha < 0$) and "In-Plane" ($2\beta_i - \beta_j - \beta_k$) C_3C– Rocking (Rocking Plane Defined by Dihedral Angle ω_i; Mean Values in Degrees; Standard Deviation σ in Parentheses)

fragment	Z	$\sum\beta - \sum\alpha$	σ	$2\beta_i - \beta_j - \beta_k$	σ	ω_i
acyclic	C_{sp^3}	10.7	(4.1)	–10.1	(4.0)	169
	C_{sp^2}	10.1	(6.6)	4.1	(7.5)	41
	P[a]	6.1	(5.2)	–11.6	(6.4)	168
	Si	10.1	(1.1)	–5.1	(3.2)	167
cyclic	C_{sp^3}	4.9	(4.5)	11.5	(4.7)	–72
	C_{sp^2}	1.8	(5.5)	–5.2	(5.0)	–87
	NH	–1.6	(5.2)	9.6	(6.4)	–80
	NMe	8.8	(1.2)	13.7	(1.3)	–74
	NS	6.1	(4.5)	7.6	(3.3)	–80
	NO	–5.4	(5.7)	2.1	(6.7)	32
	S	–6.8	(3.5)	–11.3	(2.4)	159
	O	–12.1	(5.4)			

[a] $(C_3C)_3P$ and $(C_3C)_4P$ excluded.

Despite a nonnegligible dispersion, we can do better than a case-by-case analysis and can define four major distortion modes for fragments C_3CZCC_3 ($Z = C_{sp^2}$, C_{sp^3}) as well as their probable range. They are clearly differentiated according to whether the central carbon is sp^2 or sp^3 and whether the fragment is cyclic or acyclic. The diversity of compounds with *gem*-6 behavior led us to generalize our structural observations by examining fragments C_3CZCC_3 (Z = P, N, O, S, Si).

III. General *gem*-6 C_3CZCC_3 Fragments. Distortions and Calculation of Steric Energy Resorption

The crystallographic data analysis confirms the broad outlines of our analysis of the crystallographic data of C_3CCCC_3 fragments, but interesting differences can be observed.

(30) Cossé-Barbi, A.; Massat, A. *J. Mol. Struct.* **1980**, *63*, 31.
(31) Lees, R. M.; Baker, J. G. *J. Chem. Phys.* **1968**, *48*, 5299. Tabake, K.; Kojima, T. *J. Phys. Soc. Jpn.* **1971**, *30*, 1145. Hecht, K. T.; Dennison, C. M. *J. Chem. Phys.* **1957**, *26*, 98. Tajima, K.; Nisikawa, T. *J. Phys. Soc. Jpn.* **1957**, *12*, 680. Coffey, D.; Britt, C. O.; Boggs, J. E. *J. Chem. Phys.* **1968**, *49*, 591.

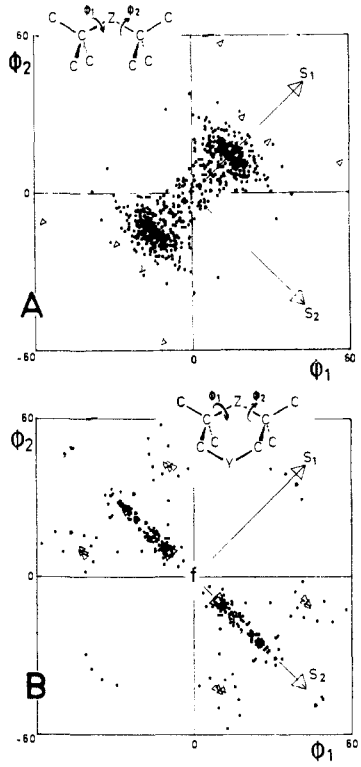

Figure 4. C_3CZCC_3 (Z = C, P, Si, N, S, O). Rotational distortion from reference f. A, acyclic fragments; B, cyclic fragments. Δ, fragment with substitutions on one or several atoms of substructures 1 or 2 ($Z \neq C$). Outliers belong to structures **18**, **51**, **106**, and **107** of the supplementary material.

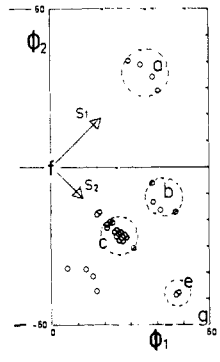

Figure 5. Rotational distortion from reference f in cyclic fragment with Z = NO: disrotatory process parallel to S_2 component (f → c, f → e) or with a dominant part of S_2 component (f → b). Twist conformers (a) are the exception (compounds **106** and **107** of the supplementary material).

III.1. Rotational Distortions. The rotational processes for avoiding gear-clashed conformers of C_{2v} symmetry are clearly differentiated according to whether the substructure is acyclic (Figure 4A) or has a six-membered ring (Figure 4B). Conrotatory processes in acyclic series and disrotatory in cyclic series are also confirmed. The range of this latter disrotatory process seems especially important for derivatives of 2,2,6,6-tetramethylpiperidine-1-oxyl (Z = NO) (Figure 5).

An interesting parallel exists between the carbon and nitrogen atoms (Table II) showing the effect of Z atom hybridization on the rotational process range. This latter is indeed larger for Z = NO (or C_{sp^2}) than for Z = NMe, NH (or C_{sp^3}). It varies according to the pyramidalization[32] of the nitrogen, equal on the average to 16° for Z = NO, 48° for Z = NMe. For Z = NO, we can invoke (diagrams 5 and 6) the role of steric interactions between oxygen 11 and equatorial substituents 7 and 9 just as for $Z = C_{sp^2}$. The need to limit this last interaction would explain why the rotation is all the more ample as pyramidalization is small.

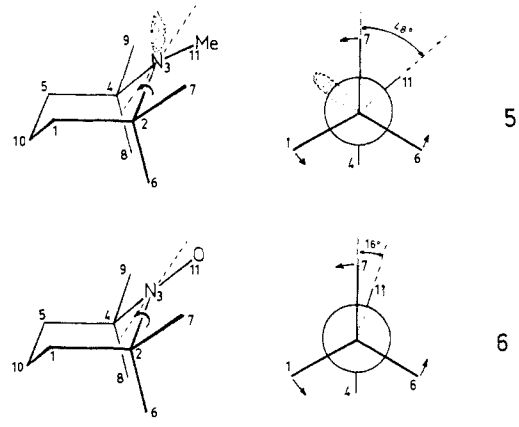

III.2. Framework distortions. (a) CZC Unit. Rotational relaxation processes are linked to very important distortions affecting valency angles CZC and, exceptionally, (as in the case of phosphorus) interatomic distances (Table III). In the latter case, and although the dominant effect concerns the CZC angle opening, we observe a tendency for the angle opening to increase (as for Z = C) for short CZ distances. This is not the case for Z = N where the CZC and CZ parameters are independent.

For Z = N, we observe no competition between rotational processes and valency opening: the angle opening is larger for Z = NO than for Z = NH, NMe, NS. The reason for the difference between Z = C and Z = N is as follows. Rotation angles are similar (26, 28°) for $Z = C_{sp^2}$ and Z = NO. In the first case, atom 11 is situated in plane 234. Its interactions with substituents 7 and 9 remain strong despite the 26° rotation (diagram 7). They prevent a significant opening of angle CZC. In

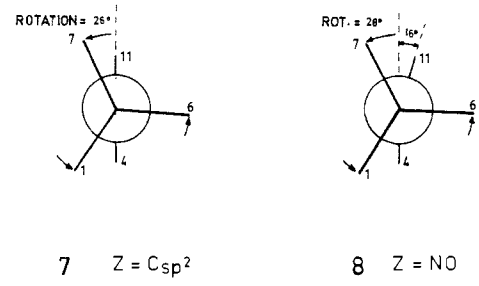

the second case, (Z = NO), with a similar rotation (28°), interactions 7–11 and 9–11 are weak (diagram 8) because of the pyramidalization of nitrogen (16°). Thus, angle CZC can open more widely.

(b) C_3C Unit. As with C_3C–C rotors, C_3C–Z rotors are very disymmetrical. Here too, the valency angles are the most affected (Table IV). The symmetry axis deviation of C_3C– rotors from the CZ bond direction is accompanied by a reduced real size of C_3C groups in acyclic series (C_3C SYM.DEF.). In cyclic series, we observe contractions for Z = NMe, NS but an expansion for Z = NO, O, S.

The detailed analysis of C_3C rocking is given in the Annex. It reveals interesting similitudes and differences with regard to the hybridization of the Z atom and the range of rotational processes.

The distortion of C_3CZCC_3 fragments, maintained despite the diversity of environments, is due to two kinds of action: rotation and frame alterations. These correspond to four types of distortion effects: rotational distortions (ROT.DST.) through conrotation (acyclic fragments) or disrotation (six-membered rings), CZC bending (CZC BEND.), CC_3 symmetrical deformation (CC_3 SYM.DEF.), and CC_3 TILT. These four strain release effects diminish the interaction of tertiary groups, both among themselves and with their neighbors, with different degrees of efficiency that we shall compare.

III.3. Contribution of the Four Strain Release Effects. The overlap exchange repulsion between the bonds or atoms is rec-

(32) Pyramidalization *P* is related to torsion angles 11 3 2 4 and 7 2 3 4 by the expression $P = |11\ 3\ 2\ 4 - 7\ 2\ 3\ 4 + 180°|$.

ognized as the principal component of steric repulsion.[21] Bond–bond repulsions predominate in little-substituted compounds, and they provoke deformations such as contraction and the tilt of methyl.[33] Atom–atom repulsions predominate in crowded systems.

The structural distortions thus result from the adaptation of the chemical system to all the bond–bond and atom–atom constraints, whether the chemical system is little substituted or crowded. The *gem*-6 systems differ in the existence of a broad CZC bending and of a fine correlated rotation not found in little-substituted systems.

Theoretical calculation can be used to ascertain whether limitation of steric energy takes place similarly in crowded and in little-substituted compounds and equally to evaluate the contribution of the four distortions to strain release.

Simulation carried out with the aid of molecular mechanics is applied to Z = C_{sp^3} and the propane case, where the structure is already distorted. The central angle is 111.38°, very near the standard gear-clashed reference (112.08°); the methyls are highly contracted (7.27°), but they exhibit no rocking. The torsion profile is unchanged. *Reduction of steric energy by optimization*[34] (–0.46 kcal·mol^{-1}) *is small.* It is obtained by diminishing the van der Waals interactions, mainly γ interactions (0.825 kcal·mol^{-1}), at the cost of E_r (0.101 kcal·mol^{-1}) and E_θ (0.21 kcal·mol^{-1}) energies linked to the bond lengths and angles *with no modification of* E_ϕ, *energy linked to torsion angles.*

In the case of 2,2,4,4-tetramethylpentane, *t*-Bu-CH_2-*t*-Bu, optimization leads to a very distorted structure of C_2 symmetry (central angle: 124.42°, rotation 13.32°, compression 10.02°, rocking –11.16°) related to the crystallographic structure. *The limitation of steric energy by optimization*[34] (–457 kcal·mol^{-1}) *is enormous.* It is obtained by a considerable reduction of van der Waals interactions (–464 kcal·mol^{-1}), at the cost of a relatively moderate increase of E_r (1.60), E_θ (4.7), and E_φ (0.78 kcal·mol^{-1}).

In van der Waals interaction reductions, two hydrogen couples (diagram 9) belonging to synaxial substituents are primarily responsible: some 200 kcal·mol^{-1} for each HH interaction.

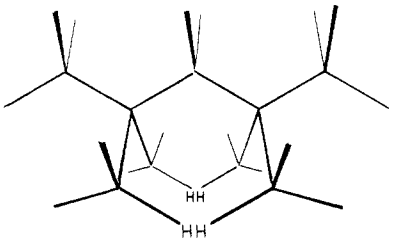

9

The various strain release effects *are not additive* (Table V). Two methods can be used to calculate their efficiency: (1) to impose one of the four effects on the reference and observe how the steric energy varies; (2) to start with a geometry deformed by the four effects and observe how the steric energy varies when one effect is eliminated.

Starting from the reference (Table V), the CZC bending brings the steric energy to 72 kcal·mol^{-1}, i.e., to 18% of its initial value (409 kcal·mol^{-1}). This simulation implies that the CZC bending could reabsorb 82% of the steric energy, if it acted alone. The torsion acting alone would bring the steric energy to 36% of its initial value, "reabsorbing" 64% of the steric energy. Contraction and rocking of tertiary groups have more modest effects. They could only reabsorb respectively 23% and 25% of the initial steric energy.

Similar results are obtained by the second method. Eliminating contraction or rocking only slightly augments the steric energy (4.4 and 4.2 kcal·mol^{-1}, respectively). The effects of torsion and, even more, of CZC bending are considerable (+13.5 and +53.7 kcal·mol^{-1}, respectively).

With molecular mechanics, the component parts of steric energy can be distributed differently according to the particular force field[35] used. The INDO method, however, leads to a comparable scale of magnitude. If the four effects cooperate, the energy reduction is 194 kcal·mol^{-1}, while each effect acting alone reduces the total energy by 177 (CZC bending), 153 (torsion), 72 (rocking), and 67 kcal·mol^{-1} (contraction).

Eliminating one of the four strain release effects on the basis of the deformed geometry leads to the same conclusions: the effects of CZC bending and of correlated rotation clearly outweigh those of rocking and of contraction.

The importance of a single factor when all four act simultaneously with varying weights undoubtedly throws light on the satisfactory results obtained historically in attempts to explain the apparent sizes by a single factor, correlated rotation.

IV. Dynamic Aspects: Interconversion Pathways

An important strain release is thus made possible by *gem*-6 structure distortions. These *also* permit a far larger conformational flexibility than in standard gear-clashed reference.

Below, we specify the interconversion mechanisms, taking into account the crystallographic results and measuring the rotation barriers by MO and MM calculation.

IV.1. Crystallographic Pathways. The dispersal of crystallographic results can serve as a basis to infer interconversion pathways between ground-state geometries, according to the structure correlation method.[36] This approach is naturally limited to the most represented subclasses Z = C, P, N for which we have a continuity between crystallographic situations.

There are two kinds of ground-state geometry. In each subclass, we observe a cluster of points for a C_2 symmetry conformer ($\phi_1 = \phi_2$) in acyclic series and for a C_s symmetry conformer ($\phi_1 = -\phi_2$) in cyclic series.

Z = C_{sp^3}, P, Acyclic Fragments. There is a gear-clashed transition state (*f*) of symmetry C_{2v} ($\phi_1 = \phi_2 = 0$) for the interconversion of gear-meshed conformers of C_2 symmetry (Figure 1). The gear slippage or conrotatory correlated interconversion pathway (axis S_1) shown[15] by fragments CC_3 C_{sp^3} CC_3 is also observed for fragments CC_3 P CC_3 (Z = C_{sp^3}, P = acyclic fragment).

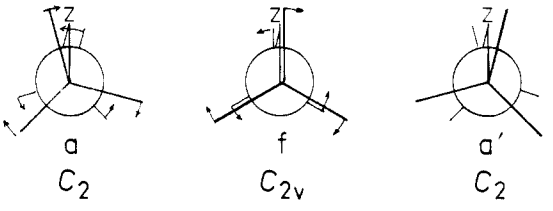

Z = C_{sp^2}. For Z = C_{sp^2} (Figure 1), the impossibility of this conrotatory *afa'* process is confirmed.[15]

Between acyclic situations (quadrants q 1, q 3) and cyclic situations (quadrants q 2, q 4), we observe a continuity (Figure 6) that may indicate a low-energy pathway or a constrained pathway.[36]

The first hypothesis implies the following: (1) A dynamic gearing disrotatory interconversion pathway *abda'* between C_2 symmetry conformers involving a transition state with very unlike rotations of the two tertiary groups. (2) A peripheral pathway

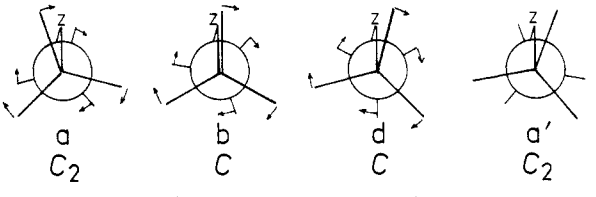

in several correlated stages associates two disrotatory stages of

(33) Flood, E.; Pulay, P.; Boggs, J. E. *J. Am. Chem. Soc.* **1977**, *99*, 5570. These authors did not point out the contraction of methyls, but this can easily be deduced from their results.

(34) Of course, the reference geometry here has the internal reference coordinates of the calculation method used (CZC = 109.93°).

(35) Lomas, J. S. *Actual. Chim.* **1976**, Mai, 7.

(36) Bürgi, H. B.; Dunitz, J. D. *Acc. Chem. Res.* **1983**, *16*, 153 and references therein.

dynamic gearing (*ab,b'a'*) parallel to the S_2 axis with a conrotatory stage of gear slippage (*bcb'*) parallel to the S_1 axis. The net result

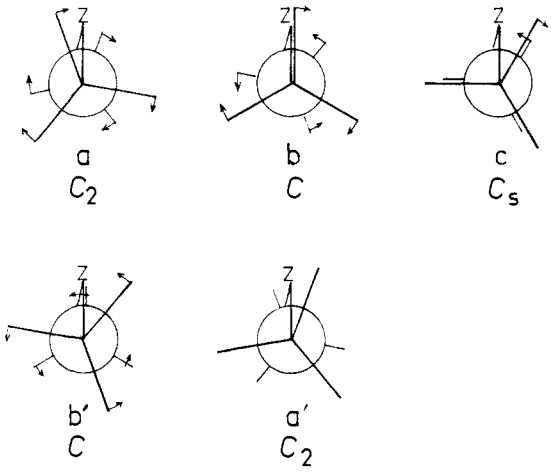

$a \rightarrow a'$ is a conrotation. This peripheral pathway is different from the noncorrelated stepwise process[14] revealed in other crowded compounds. In these, each rotor, in turn, turns alone while the other is halted. It also differs from the peripheral mechanisms we described in anomeric compounds,[37] which associate two disrotatory correlated stages with one noncorrelated stage.

Z = NO (Cyclic Fragments). The continuity here is not excellent (Figure 5). However, the existence of a structure *e* of C_s symmetry ($\Phi_1 = -\Phi_2 \simeq 50°$) with strong tertiary group rotation indicates the possibility of a disrotatory interconversion pathway (S_2 axis) between gear-clashed ground-state conformers of C_s symmetry. This pathway would allow one transition state (*g*) with a locally planar cycle ($\phi_1 = -\phi_2 = 60°$). Given the gradual pyramidalization of the nitrogen atom, associated with ϕ_i torsion (section III.1), we can represent this mechanism as follows:

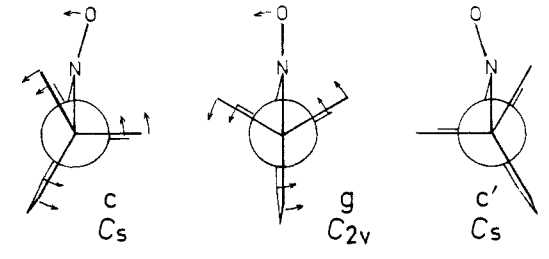

These various mechanisms were tested by simulations with MM 2 (Z = C_{sp^3}) or by MO calculation (Z = C_{sp^2}, NO). For Z = C_{sp^3}, we confirm (Figure 7A) the conrotatory process. The associated energy, 0.81 kcal·mol^{-1}, is very close to that calculated by Bürgi and co-workers.[23] For Z = C_{sp^2} (Figure 6B), the disrotatory *abda'* and peripheral *abcb'a'* mechanisms require, respectively, 1.28 and 2.54 kcal·mol^{-1}. The conrotatory mechanism would require 3.73 kcal·mol^{-1}. For Z = NO (Figure 7B), the disrotatory process *cgc'*, admitting a locally plane transition state, seems more probable than the disrotatory process *cfc'* admitting a chair structure for the transition state (2.43 vs 2.82 kcal·mol^{-1}).

The energies associated with the interconversion processes are very *moderate*. Such small barriers in such crowded compounds are indeed surprising, and we are led to wonder whether the framework deformation does not play an important part in lowering the rotation barrier.

IV.2. Interconversion Barriers and Framework Distortion. At first glance, the energy surface of little-substituted compounds has as many dimensions as torsion angles ϕ_i. The conformational map is seen as a slightly undulating space, all of whose parts can be comparably explored by the molecule (Boltzmann factors of approximately similar sizes).

When the strain increases, the energy hypersurface E (r_i, θ_i, ϕ_i) becomes more complex. It has as many dimensions as it has linearly independent internal coordinates. The conformational map E (ϕ_i) then represents the energy value for parameters r_i and θ_i that minimize E for any combination of ϕ_i's.

Given such complexity, we decided to evaluate the perturbation of the conformational map caused by framework distortion for *gem*-persubstituted compounds.

This link between framework distortion and conformational flexibility is established in the present paper as well as in other work.[38] In order to approach these perturbation effects, we compare the conformational maps of the 2,2,4,4-tetramethylpentanone (*t*-Bu-CO-*t*-Bu) obtained with a standard and an optimized framework. The following elements appear: (1) Framework distortion acts as a powerful erosion mechanism smoothing the rough surfaces of the map. The total energy variation changes from 140 kcal·mol^{-1} in standard geometry to $\simeq$4 kcal·mol^{-1} in optimized geometry. (2) Relatively high energy zones are maintained (4 kcal·mol^{-1}). The molecule no longer explores the whole of the conformational map (Boltzmann factors of a different approximate size). (3) Interconversion energies are nonetheless situated within reasonable limits because they adopt the narrow valleys or gorges that criss-cross an uneven landscape. The specific rotational processes, a mainly disrotatory process *abda'*, a peripheral process *abcb'a'*, are close to pathways inferred from crystallographic data.

Framework distortion attenuates the disrotatory process energy (from 51 to 1.28 kcal·mol^{-1}) and reveals the peripheral process (2.54 kcal·mol^{-1}). These two processes are stabilized at the expense of the *afa'* conrotatory process whose energy increases (from 2.23 to 3.73 kcal·mol^{-1}).

These remarks are valid for compounds where Z = C_{sp^3} and NO (Figure 7); conrotatory process energy (Z = C_{sp^3}) and disrotatory process energy (Z = NO) are prohibitive—respectively 400 and 120 kcal·mol^{-1}—in the absence of framework deformation.

It is, therefore, indeed framework distortion that enables us to measure (e.g., in IR) the energy of specific rotational mechanisms with two or more rotors. Without framework deformation, these mechanisms would remain unrevealed.

Conclusion

Crystallographic data analysis of C_3CZCC_3 fragments provide a structural support for interpreting the *gem*-6 effect once we circumscribed the use of a standard molecular framework model.

The interplay of correlated rotation with bond angle deformation is an important characteristic of crowded molecules, since simulations using crystallographic results and theoretical hypersurfaces of energy reveal considerable conformational flexibility due to important lowering of rotation barriers associated with deformations of the molecular framework.

Methods and conclusions utilized herein provide a sound basis for the study of reactivity maps of congested systems.

Annex—Analysis of the C_3C–Z Tilt

In CH_3XH compounds, the methyl tilt has been interpreted as a combination of bond–bond repulsions and bond–lone pair repulsions.[33] We show here that the direction and the amplitude of the rocking make it possible to estimate the dominant bond–bond and atom–atom interaction in the C_3CZCC_3 fragments studied. We note the following:

(1) In Acyclic Series, A Similarity between C_{sp^3}, Si, and P. The tilt is symmetrical with regard to a plane next to that of CZC. It tends to separate from each other, on the one hand, synaxial groups 1 and 5, and on the other hand, 6 and 8. Therefore, the bond–bond and atom–atom interactions related to the proximity of these groups are dominant. They are indeed clearly equal, since the average rotations of both C_3C groups are small. The difference is quite clear with the case of Z = C_{sp^2}, where the rocking plane ($\omega_i \simeq 40°$) indicates the dominance of the interactions linked with the proximity of only two synaxial groups (1 and 8) (Figure 2). Indeed, the four synaxial groups are no longer equivalent because of the more ample correlated rotation in this case (a 20° average).

(37) Cossé-Barbi, A.; Dubois, J. E. *Tetrahedron Lett.* **1986**, *27*, 3501; *J. Am. Chem. Soc.* **1987**, *109*, 1503.

(38) Cossé-Barbi, A.; Massat, A.; Dubois, J. E. *Bull. Soc. Chim. Belg.* **1985**, *94*, 919.

Table V. Contribution of the Four Strain Release Effects, Simulation MM2. (Distortions in Degrees; Steric Energy E_{st} and van der Waals E_{HH} Energy in Kilocalories/Mole; r_{HH} Distance in Angstroms)

geometry	torsion	∠CZC	rocking	contraction	E_{st}	E_{HH}	r_{HH}
optimized	13.316	124.425	−11.16	10.02	15.07	0.46	2.20
formal reference	0	111.383[a]	0	0	409.5	175	0.75
contraction alone	0	111.383	0	10.02	316.7	135	0.85
rocking alone	0	111.383	−11.16	0	306.3	131	0.86
torsion alone	13.316	111.383	0	0	145.6	42	1.24
CZC bending alone	0	124.425	0	0	72.1	26	1.29
contraction + rocking	0	113.383	−11.16	10.02	224	94	0.96
CZC bending + torsion	13.316	124.425	0	0	35.5	7	1.64
four effects	13.316	124.425	−11.16	10.02	24.5[b]	3.1	1.82
without contraction	13.316	124.425	−11.16	0	28.9	4.6	1.74
without rocking	13.316	124.425	0	10.02	28.7	4.8	1.73
without torsion	0	124.425	−11.16	10.02	38.0	10.6	1.51
without CZC bending	13.316	111.383	−11.16	10.02	83.2	23	1.38

[a] Value from propane optimization. [b] Different from the optimized energy because of the optimization of other parameters (bond lengths, CCH bond angles, CCCH torsion angles).

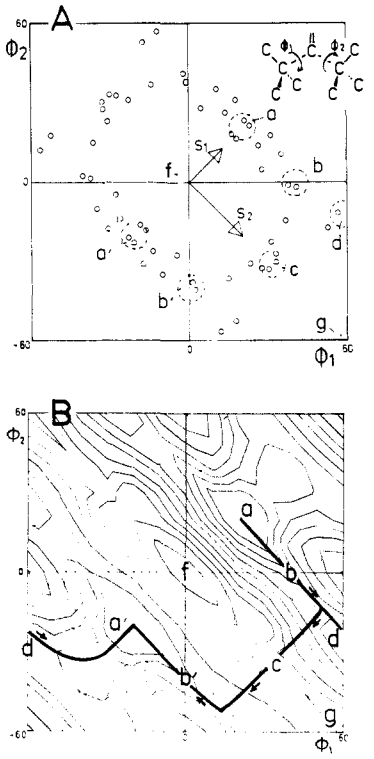

Figure 6. Interconversion mechanisms $a \rightarrow a'$ (Z = C_{sp^2}, acyclic fragments): A, crystallographic results (above); B, INDO calculation, optimized geometry (below).

(2) In Cyclic Series, An Analogy between NMe, NS, and C_{sp^3}. The tilt takes place symmetrically with regard to each of the two ZCC planes ($|\omega_i| \simeq 75°$) containing both synaxial carbons. It tends to separate the two interactive synaxial groups 6 and 8 (diagrams 4 and 5). The repulsion interaction associated with the two synaxial substituents is thus greater than the repulsion interactions that result from the proximity of equatorial groups and Z atom substituents.

(3) In Cyclic Series, A Clear Difference between Z = C_{sp^2} and Z = NO. For Z = NO, CC_3 groups expand, and there is no rocking effect. Rotational relaxation (28° average), associated with a large angle opening and nitrogen pyramidalization ($\simeq 16°$), is able to suppress at once the synaxial interactions 6/8, the 11/7 (diagram 8) and 11/9 interactions of the oxygen atom with equatorial substituents, and the associated bond–bond interactions. This is not the case for Z = C_{sp^2} where a reverse tilt (negative rocking coordinate) reveals the predominance of repulsion interactions linked to the proximity of equatorial groups (7, 9) and Z atom substituents (C, N, O) (diagram 7). Thus, for Z = C_{sp^2} and Z = NO, despite similar large rotation angles (26–28°) (diagrams 7 and 8), the strain release of the former is partly inhibited due to the absence of pyramidalization of the C_{sp^2}.

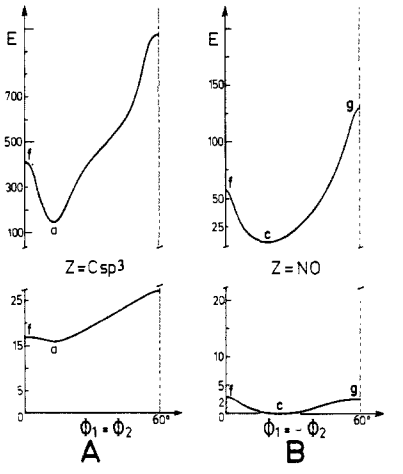

Figure 7. Conformational flexibility and framework distortion: A, along the conrotatory S_1 coordinate (Z = C_{sp^3}; MM2 calculation); B, along the disrotatory S_2 coordinate (Z = NO; INDO calculation). Energies calculated in kcal·mol^{-1}, given the hypothesis of a rigid skeleton (above), of a deformable skeleton (below). A change of scale was needed for the energy variation in this second hypothesis to be seen.

(4) An Analogous Situation for Z = S and Z = O. C_3C groups expand, and we observe a very important rocking effect allowing the CZC plane as a symmetry plane. Clearly, no strong interaction (7–11, 7–12, 9–11, 9–12) implying equatorial positions 11 and 12 counterbalances those interactions linked to the proximity of synaxial groups 6 and 8 (diagram 10). As in little-substituted compounds (CH_3OH),[33] the bond–lone pair repulsion interactions (7–11, 7–12, 9–11, 9–12) prove small.

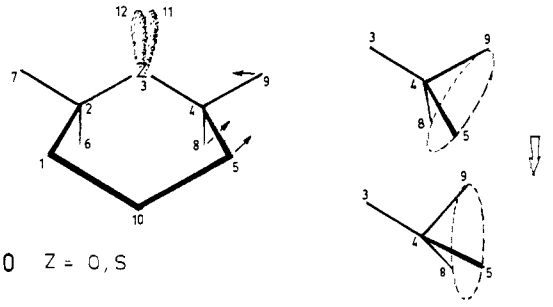

Like CZC bending and the correlated rotation of C_3C groups, rocking contributes then to diminish the apparent size of tertiary groups, i.e., to limit their interactions with their neighbors.

Registry No. C_3COCC_3, 77887-46-8; C_3CSCC_3, 78050-22-3; C_3CNOCC_3, 2564-83-2; $C_3CNMeCC_3$, 79-55-0; C_3CNHCC_3, 768-66-1; *t*-Bu-CH_2-*t*-Bu, 1070-87-7; *t*-Bu-CO-*t*-Bu, 815-24-7.

Supplementary Material Available: Lists of cyclic and acyclic fragments from the Cambridge Data Base (5 pages). Ordering information is given on any current masthead page.